Sustainable Cities and Society 82 (2022) 103882

Contents lists available at ScienceDirect

Sustainable Cities and Society

journal homepage: www.elsevier.com/locate/scs

How do disparate urbanization and climate change imprint on urban thermal variations? A comparison between two dynamic cities in Southeast Asia

Can Trong Nguyen [a,b,*], Amnat Chidthaisong [a,b,*], Atsamon Limsakul [c], Pariwate Varnakovida [d], Chaiwat Ekkawatpanit [e], Phan Kieu Diem [f], Nguyen Thi Hong Diep [f]

[a] The Joint Graduate School of Energy and Environment, King Mongkut's University of Technology Thonburi (KMUTT), Bangkok 10140, Thailand
[b] Center of Excellence on Energy Technology and Environment (CEE), PERDO, Ministry of Higher Education, Science, Research and Innovation, Bangkok 10140, Thailand
[c] Environmental Research and Training Center, Technopolis, Klong 5, Klong Luang, Pathumthani 12120, Thailand
[d] KMUTT Geospatial Engineering and Innovation Center (KGEO), Department of Mathematics, Faculty of Science, King Mongkut's University of Technology Thonburi (KMUTT), Bangkok 10140, Thailand
[e] Civil Engineering Department, Faculty of Engineering, King Mongkut's University of Technology Thonburi (KMUTT), Bangkok 10140, Thailand
[f] College of Environment and Natural Resources, Can Tho University, Can Tho City, Vietnam

ARTICLE INFO

Keywords:
Climate change
Land surface temperature
Rapid urbanization
Temperature extreme
Urban heat island

ABSTRACT

This study assessed the combined influences of climate change and urbanization on land surface temperature (LST) and surface urban heat island (SUHI) in the Bangkok metropolitan region (BKK) and Ho Chi Minh City metropolitan area (HCM) during 1990–2020. We found climate change evidence from trends and variations of temperature extremes in both cities throughout the past three decades, especially for the significant upward trends of nighttime temperature in HCM (0.23 – 0.3 °C/decade). These cities have been undergoing rapid urbanization, in which HCM has a higher urbanization rate with an annual growth rate of 8.03%/year against BKK (4.26%/year). Landscape metrics have rapidly shifted towards urban aggregation and green space fragmentation along with urbanization. A peer comparison shows that BKK holds a greater urban size and LST intensity, while HCM leads in urban growth and SUHI magnitude. These changes jointly contribute to climbing SUHI intensity, especially the dramatic influence of surface changes. Yet, temperature extremes also play an indispensable role in regulating SUHI magnitude, in which the impact in HCM is considerable compared to the effect in BKK. The research findings provide crucial information for both cities – where incorporation of climate change resilience strategies and SUHI mitigation into the master plans for livable cities are recommended.

1. Introduction

Since the middle of the twentieth century, Thailand's Bangkok metropolitan region (BKK) and Vietnam's Ho Chi Minh City metropolitan area (HCM) have seen significant urbanization, with impressive economic growth rates and urban population increases. Although urbanization facilitates intensive needs for general development, it also induces a slew of issues, ranging from unemployment to urban poverty, social division, and environmental degradation. Urbanization is inextricably linked to urban agglomeration, and LULC (land use/land cover) changes (Estoque & Murayama, 2015; Min et al., 2018). Natural landscapes and agricultural fields, for example, are increasingly encroached upon by urban characteristics such as transport infrastructures, buildings, and residential areas. Physically, these urban features are made of low albedo materials and impermeable surfaces, which absorb more solar radiation and reduce evaporation. As a result, urbanization is frequently referred to as a major contributor to the formation of surface urban heat island (SUHI) (Khamchiangta & Dhakal, 2019)—a microclimate phenomenon that describes the differential temperature between urban and rural areas (US EPA, 2008c). SUHI has also been linked to residents' discomfort, heat-related morbidity, and mortality (Lowe, 2016; Santamouris, 2020), as well as increased energy consumption from cooling demand (Nguyen et al., 2021). It is especially hazardous to the elderly, disabled, and low-income individuals in the summer and during heatwaves (Santamouris, 2020).

* Corresponding authors: 126 Pracha Uthit Rd., Bangmod, Thung Khru, Bangkok 10140, Thailand.
E-mail addresses: can.62300800201@mail.kmutt.ac.th (C.T. Nguyen), amnat.chi@mail.kmutt.ac.th (A. Chidthaisong).

https://doi.org/10.1016/j.scs.2022.103882
Received 10 September 2021; Received in revised form 1 April 2022; Accepted 1 April 2022
Available online 5 April 2022
2210-6707/© 2022 Elsevier Ltd. All rights reserved.

List of abbreviations and acronyms

AI	Aggregation index
AUGR	Annual urban growth rate
BKK	Bangkok metropolitan region
GEE	Google earth engine
HCM	Ho Chi Minh City metropolitan area
LPI	Largest patch index
LSR	Land surface reflectance
LST	Land surface temperature
LULC	Land use/land cover
MBI	Modified Bare soil Index
MKA	Mann-Kendall analysis
MNDWI	Modified Normalized Difference Water Index
MOT	Multiple Otsu Threshold
NDVI	Normalized Difference Vegetation Index
NP	Number of patches
PCA	Principle component analysis
PLAND	Percentage of landscape
SEA	Southeast Asian
SUHI	Surface urban heat island
SUHII	Surface urban heat island intensity
SVM	Support vector machine
TN	Minimum air temperature
TNMEAN	Average value of minimum air temperature
TNN	Minimum value of minimum air temperature
TNX	Maximum value of minimum air temperature
TX	Maximum air temperature
TXMEAN	Average value of maximum air temperature
TXN	Minimum value of maximum air temperature
TXX	Maximum value of maximum air temperature
UHI	Urban heat island
UI	Urban Index

With global warming and further urban development in both cities, the SUHI condition is likely to deteriorate. BKK, in particular, has expanded its urban areas to neighboring provinces and connected to the Eastern Economic Corridor, a national initiative spanning three coastal provinces east of BKK that aims to progressively transform Thailand into a developed country (Can et al., 2021). HCM, on the other hand, has grown and connected its main city to outlying "satellite cities". By 2030, it is anticipated to be the next regional megacity (United Nations, 2018). Because they are both located on the Belt and Road Initiative (BRI) routes, a strategy to improve and enhance the world's trade among Eurasian continental countries, urbanization in BKK and HCM will be significantly accelerated and more dynamic than ever before (Ascensão et al., 2018). These cities will gradually lose the critical self-cooling capacity of blue spaces (e.g., rivers, lakes, wetlands) and green spaces (e.g., parks, lawns, shrubland) due to replacement with man-made constructions (Cheng et al., 2019; Davtalab et al., 2020). In addition to changing the urban landscape and materials, dynamic urbanization also profoundly alters urban morphology, which ultimately aggravates or alleviates SUHI in a city depending on the city-scale, urbanization level, and considered time. Typically, urbanization in fast-developing countries induces SUHI due to the escalation of heat-absorbing materials and unplanned constructions to ensure standards on urban green spaces, ventilation, street width, distance between individual buildings, and building height. When the standards for these constructive distances are not satisfied, it reduces urban ventilation and sky-view factor (SVF) restricting outgoing radiation and circulation of cool winds into cities to mitigate the urban heat island (UHI), especially during nighttime (He et al., 2020). However, high-rise buildings can contribute to UHI mitigation by shading the shadowed sides during the daytime as urban trees do to cool down temperatures (Harun et al., 2020).

Southeast Asia (SEA) is recognized as one of the most vulnerable regions to climate change (Akhtar, 2016), and climate change will exacerbate the SUHI impacts (Iping et al., 2019). According to IPCC (Intergovernmental Panel on Climate Change), the global temperature has increased by nearly 1.0 °C since the Industrial Revolution (Henderson et al., 2018; National Research Council, 2012). Without reducing greenhouse gas emissions, the world's temperature rise will quickly reach 1.5 °C by 2030 and 2.0 °C by 2060 (IPCC, 2018). It means urban temperature and SUHI will increase further because of the integrative impact of continuing urban expansion and global warming. As a result, the urban areas and their inhabitants will become more vulnerable to global and local threats. Nevertheless, Chapman et al., (2017) indicated in a review article that only 14% of the existing studies assessed both urban expansion and climate change interactions on land surface temperature (LST) and SUHI. Therefore, there is an urgent need to better understand the relationships between climate change, urbanization, and the impacts on SUHI.

To date, many studies have investigated the thermal environment changes in BKK (Estoque et al., 2017; Khamchiangta & Dhakal, 2019; Srivanit, 2012). These studies provide a wide range of knowledge from general increase LST induced by urbanization, the influence of urban morphology, and physical and non-physical factors. Similar research in HCM has studied both LST changes and SUHI (Quang et al., 2016; Son et al., 2017; Van et al., 2017). In general, the studies found upward trends of LST and SUHI with proportional relationships with the urbanization process. Nevertheless, these studies have been considered independently in each city using unique methodologies during different periods. For instance, most research was limited to inside the administrative boundaries, while urban sprawl, especially in SEA, is often not confined to administrative boundaries but spreads out along the transport system. Therefore, it leads to inadequate assessment regarding urbanization for a city. The study area definition is also crucial for remote sensing-based SUHI intensity (SUHII) calculation, as it influences the estimated average temperature of rural and urban areas.

There are two different views with regards to LST analysis; the first one is focused on temperature variations over a prolonged period of time, while the second is focused on connections between LST and surface characteristics at a single point in time. In addition, landscape measurements and urban morphology are frequently overlooked when the studies are carried out in HCM (Van & Bao, 2015). As a result, comparing the rate of urbanization and the intensity of SUHI between the two cities using outputs from previous studies is challenging. Therefore, a peer-to-peer comparison of the two cities should be conducted using a consistent methodological framework, research duration, and focus area. It will be useful for cross-city comparisons to understand the SUHI of each city better, as well as to learn from the practical lessons of sustainable development.

Driven by the statements and research gaps above, we implemented this study to bridge the knowledge gaps related to the combined impacts of climate change and urbanization on SUHI and consolidate the present knowledge pool related to factors affecting SUHI. Reanalysis data was adopted for climate change analysis to limit interactions and combined effects often found in observation data. The relevance of climate change to urban thermal environmental shifts was also included. Specifically, this study investigated the changes in temperature extremes as a typical aspect of climate change in the two cities during the past 30 years. The urban expansion and its induced impacts on landscape alterations and variation in LST and SUHI were then explored. Ultimately, we analyzed and compared how urbanization and climate change factors divergently contribute to the thermal environment in each city. With respect to these

cities, the research findings are expected to be useful for urban developments regarding climate change impacts, urbanization, urban landscape characteristics, and stresses under SUHI. Furthermore, the core elements controlling the SUHI of each city will be vital for regulating and mitigating urban climate extremes toward more sustainable and livable cities.

2. Study areas and data acquisition

2.1. Study areas

The focus locations in this study are Bangkok metropolitan region (BKK), Thailand, and Ho Chi Minh City metropolitan area (HCM), Vietnam. BKK and HCM are located on the Indochinese Peninsula mainland (Fig. 1A), the two critical nodes in the Southeast Asia (SEA) megacity network. BKK is Thailand's capital and a national socioeconomic magnet. With over 10.2 million dwellers (2018), BKK holds third place in SEA's biggest megacities after Manila and Jakarta (United Nations, 2018). It is under the tropical savanna climate in the Köppen-Geiger climate classification system, with the influence of seasonal monsoon winds (i.e., southwest monsoon and northeast monsoon) (Bimaganbetova et al., 2020). There are three distinct seasons in BKK, the rainy (June–October), winter (November–February), and summer season (March–May) (TMD 2015). During the summer season, the average temperature is about 34 °C, and the highest temperature can reach 39–40 °C in April (Pakarnseree et al., 2018).

HCM is located in the southeastern part of Vietnam in a relatively flat region. HCM has a tropical savanna climate affected by the wet and dry monsoon. The climate is divided into two seasons, wet season (May–November) and dry season (December–April) (Quang et al., 2016). The average temperature during the dry season is approximately 30 °C, and the highest temperature is also reached in April—known as the "HCM summer" (Dang et al., 2019). Although HCM is not a capital city, it is the most dynamic center in Vietnam regarding socioeconomic and entertainment activities. Development started in the 1980s under the economic reform of the Doi Moi policy. After this renovation policy, HCM has had remarkable transformations in urbanization, economy, environment, and society (Fig. 1B) (Fan et al., 2019). The population of HCM was about 8.2 million inhabitants in 2018 (United Nations, 2019). It should, therefore, be a megacity by 2030.

In general, BKK and HCM are both located on a coastal plain and dominated by the same climate zone. Both cities are embraced by natural sceneries and have a river flowing through them, so they are both cooled down by these green-blue spaces, and natural atmosphere circulation (i.e., sea-land breezes). Therefore, the different patterns and rate of urban developments between the two cities can provide valuable information on the imprints of urbanization on urban thermal variation. Doing this also requires a comparable boundary. The metropolitan region definitions of BKK and HCM are diverse and varied among different perspectives. For instance, most studies consider the BKK region as an extensive region including Bangkok and five surrounding provinces. However, other studies define the BKK region as a smaller provincial cluster with only Bangkok and the two nearest provinces in the North and South (Can et al., 2019; Nguyen et al., 2021). These facts also apply for the HCM region scope when it is investigated under diverse research limits and objectives. Therefore, to work towards an even comparison between the two metropolitan regions in this study, we designed the study area as a buffer zone covering 30-km from each city center.

2.2. Air temperature data

We used the TerraClimate dataset available on the Google Earth Engine platform (GEE) to obtain monthly maximum temperature (TX) and monthly minimum temperature (TN) in this study. TerraClimate is a meteorology and climatic water balance dataset at monthly temporal resolution and approximately 4-km spatial resolution, which is relatively better than other current climatic reanalysis data (Abatzoglou et al., 2018). It is produced by climatically aided interpolation, which combines high spatial resolution data from the WorldClim dataset with finer temporal data from CRU Ts4.0 and the Japanese 55-year

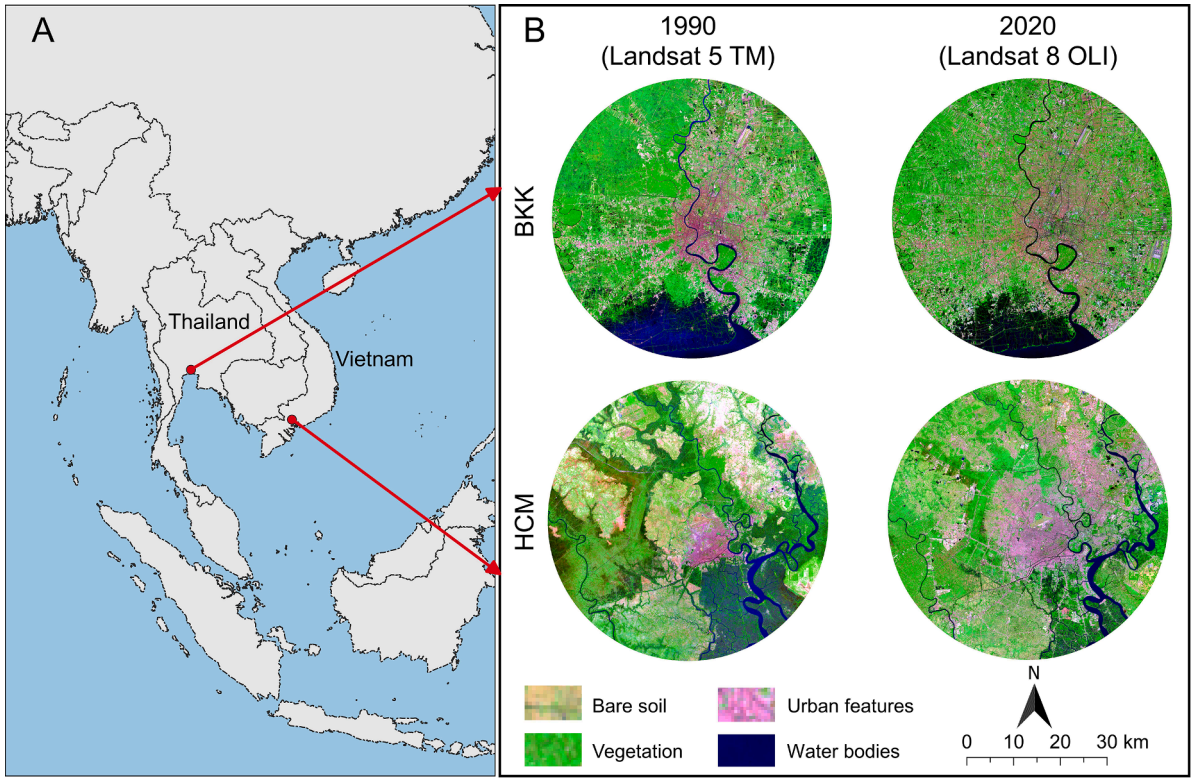

Fig. 1. (A) Location of BKK and HCM, and (B) Landsat imagery captured in 1990 and 2020 in BKK and HCM. Image false-color composite (RGB: SWIR2-NIR-GREEN).

Reanalysis (JRA55). The output of this combination method achieves better spatiotemporal resolution with strong validation compared to station-based observations. It is therefore recommended to utilize for long-term assessment in climate-related analyses that require time-varying and high spatiotemporal resolution (Artola et al., 2020). The typical studies standing on TerraClimate data can be found at Susanti et al. (2021) and Berliana et al. (2021). In addition to spatial and temporal properties, we adopted the TerraClimate instead of meteorological observation data because the observation captures combined effects from general climate conditions and human-caused disturbances, here as urban expansion. In comparison, reanalysis data are generated from meteorological models based on natural atmospheric circulations rather than surface processes (Fall et al., 2010; Yaung et al., 2021). The reanalysis data were thus applied to limit the effects of urbanization on general climate considerations within this study. We acquired monthly maximum and minimum temperatures over the past thirty years (1990 – 2020) as initial data before procedures of data quality and assessments regarding extreme climate variabilities were implemented. The data at each five-year milestone corresponding to land use/land cover data served for analysis to find associations between urbanization and climate variations.

2.3. Free-cloud composite of Landsat surface reflectance

Landsat surface reflectance (LSR) products (Collection 1, Tier 1) of Landsat 5 (TM) and Landsat 8 (OLI) were used for this study. LSR data have been atmospherically corrected using Landsat Ecosystem Disturbance Adaptive Processing System (LEDAPS) and Landsat surface reflectance code (LaSRC) for Landsat 4–7 and Landsat 8, respectively. Top of atmosphere (TOA) and brightness temperature (BT) were generated from calibration parameters. These products were then combined with other auxiliary data to generate LSR products. LSR measures the fraction of reflected solar radiation from the target objects. It depends less on sensors and weather conditions. Therefore, LSR is utilized for long-term period applications with different sensors. Annual clear-sky composites were aggregated from images taken within a year. Cloudy pixels were masked by pixel quality values, a property attached along with the LSR product generated from the CFMask (C-Function of Mask) algorithm. This study obtained images at seven time-hooks with a five-year interval, starting from 1990 until 2020.

3. Methods

3.1. Temperature extreme indices and temperature trend analysis

Climate change contributes to increasing intensity and frequency of extreme climate events. Therefore, it is able to be detected by extreme changes over a long-term period (Knutson et al., 2017). This study utilized six extreme temperature indices (i.e., “second-level indices”), which were annual indicators synthesized by monthly maximum and minimum temperatures based on the concept of Climate Change Indices proposed by the expert team on climate change detection and indices (ETCCDI) (Zhang, 2009). These temperature indices were adopted for temperature trend analysis as these are the most fundamental aspects of daytime and nighttime temperatures. Firstly, the original data went through a set of cleaning procedures presented by Sein et al., (2018). TX and TN were checked for internal consistency, temporal outliers, and data homogeneity. After passing through these quality tests, six temperature-related indices were calculated (Table 1).

The climate trends were then analyzed using Mann-Kendall analysis (MKA) (Kendall, 1975; Mann, 1945). Finally, the trend magnitude was quantified by the Thiel-Sen slope (Sein et al., 2018). The MKA aims to test whether a dataframe has a statistically monotonic trend throughout time, even nonlinear movement. Ordinary linear regression is interpretable and straightforward, but it strictly requires data uniformity of normal distribution. Yet, the MKA is a nonparametric method, which is applicable for even a free-distribution dataframe. Hence, the MKA is broadly applied in climate studies to recognize significant climate shifts (Güçlü, 2018).

Table 1
Temperature extreme indices adopted in this analysis.

Temperature index	Definition	Unit
TNMEAN	Annual average value of monthly minimum temperature	°C
TNN	Annual minimum value of monthly minimum temperature	°C
TNX	Annual maximum value of monthly minimum temperature	°C
TXMEAN	Annual average value of monthly maximum temperature	°C
TXN	Annual minimum value of monthly maximum temperature	°C
TXX	Annual maximum value of monthly maximum temperature	°C

3.2. Mapping land use/land cover using support vector machine classifier

3.2.1. Preprocessing

Firstly, yearly free-cloud composite images were generated at seven-time hooks starting from 1990 with a five-year interval on Google Earth Engine Platform (GEE). Cloud and cloud shadow pixels were masked out for each image using bit-mapped values within the quality assessment (QA) band (Foga et al., 2017). An annual cloudless image was then composited from the images within a year based on the median operator. Subsequently, the composite images were cropped following the buffer zones defined for each city as presented in Section 2.1.

3.2.2. Automatic sampling

Training data for satellite image classification is often from the field survey, which assists in collecting LULC locations by GPS device. It is a costly mission, especially when we have several remote study sites. State-of-the-art studies have applied the “show historical imagery” tool on Google Earth to acquire samples for training and validation in the past (Kostianoy et al., 2020). It has time constraints because truth point sets are manually marked, and it needs to be updated for another year. This is an arduous task when mapping time series data for a few decades.

For these reasons, we proposed an automatic sampling approach based on the image’s data itself and the “confident areas”, zoned by spectral indices and thresholding methods. Firstly, we calculated four spectral indices representing the primary land cover types. Specifically, vegetation is able to be detected by normalized difference vegetation index (NDVI) (Tucker, 1979). Water bodies were extracted by modified normalized difference water index (MNDWI), introduced by Xu (2006), as an optimal solution to identify water surfaces, especially in urban areas. Bare soil and built-up features are often misclassified because they have similar spectral characteristics (Diep et al., 2019). Therefore, bare soil was extracted by modified bare soil index (MBI), as introduced by Nguyen et al., (2021) for a tropical region like SEA. To detect urban features, we applied urban index (UI) by a normalized ratio between Shortwave Infrared band 2 (SWIR2) and Near Infrared (NIR) (Kawamura et al., 1996). All the equations of spectral indices are shown as follows:

$$NDVI = \frac{NIR - Red}{NIR + Red} \tag{1}$$

$$MNDWI = \frac{Green - SWIR1}{Green + SWIR1} \tag{2}$$

$$MBI = \frac{SWIR1 - SWIR2 - NIR}{SWIR1 + SWIR2 + NIR} + f \tag{3}$$

$$UI = \frac{SWIR2 - NIR}{SWIR2 + NIR} \quad (4)$$

where, *Green* is visible green wavelength (0.52–0.60 μm); *Red* is the visible red wavelength (0.63–0.69 μm); *NIR* is Near Infrared (0.76–0.90 μm); *SWIR1* and *SWIR2* are Shortwave Infrared bands which stand from 1.55 to 1.75 μm and 2.09 to 2.35 μm on the electromagnetic spectrum, respectively; *f* is an additional factor ($f = 0.5$).

Subsequently, the confident land cover areas were identified to construct binary images by four spectral indices using a conventional decision tree model and threshold values. The threshold values were obtained from Multi-Otsu Thresholding (MOT – Otsu, 1979). Isolated pixels and small groups of pixels were eliminated to limit potential noise effects and increase confidence. The binary images were then adopted as the background for random pixel selection. The sample size for each land cover was determined in a range from the minimum number of actual pixels up to 2,000 pixels, which is equal to five times the samples for a limited population suggested by the Taro Yamane equation (~400) (Yamane, 1967). This sample size is considered sufficient for classifying an approximate 2,800-km^2 region compared to field data and manual sampling.

3.2.3. Support vector machine classification

Machine learning-based classifiers (MLC) have gained recognition in their roles as LULC classifiers in the last few years. Among the MLC, random forest (RF) and support vector machine (SVM) are the two most applied classifiers. Noi et al. (2018) stated that classification accuracy using SVM exceeds RF, and is less dependent on sample size. It was proved through our trial classifications that urban areas generated by SVM were more stable over time compared to the RF outputs. Thus, we decided to apply SVM to classify the LULC maps for the study sites. The classifier was trained for 70% of the truth points, whereas the remaining dataset was used to validate and assess the classification accuracy. There were six bands (visible bands, NIR, SWIR1, and SWIR2) and four spectral indices contributing to model training as predictor variables. The values at reference pixels were then extracted to train the classifier and evaluate model performance. Finally, the classification was evaluated by estimating overall accuracy and kappa coefficient commonly used to assess remote sensing classification (Congalton & Green, 2009).

3.3. Landscape metrics and urbanization assessment

This study applied landscape metrics representing fragmentation and aggregation of urban features and green space patches to evaluate and compare the urbanization process between the two cities. Specifically, we selected four landscape metrics consisting of a percentage of landscape (PLAND), aggregation index (AI), largest patch index (LPI), and number of patches (NP) for our analyses (McGarigal et al., 2012; Table 2).

Urbanization was basically assessed by changes in urban density and annual urban growth rate (AUGR). Urban density is the percentage of the urban area in the total area. AUGR is an indicator for evaluating urbanization speed, which measures the yearly average urban gain ratio (Hong Diep et al., 2021). On the other hand, urbanization patterns were analyzed by the urban landscape analysis tool (ULAT) (Parent, 2009). The tool classifies the urbanization areas into three classes corresponding to three urbanization patterns of infill, extension, and leapfrog forms. Infill urbanization is a new urban area just emerging among the old urban areas. The extension form is a new urban area developed at the fringe of the already developed urban areas. In contrast, the leapfrog pattern develops separately outside urban areas in the rural areas.

3.4. Estimating daytime LST and SUHI intensity

We obtained daytime LST (at 10:30 am local time) using a widely applied algorithm, which converts DN values to LST by calibrating brightness temperature (T_B) using NVDI-based land surface emissivity (LSE) (Eq. (7)). Firstly, vegetation fraction (FVC) was calculated by calibrating specific NDVI pixel by NDVI values of fully dense vegetation ($NDVI_V$) and completely bare soil surface ($NDVI_S$) (Eq. (5)) (Carlson & Ripley, 1997). Practically, many studies used minimum NDVI and maximum NDVI values to represent $NDVI_S$ and $NDVI_V$. Yet, the minimum NDVI value belongs to the water surface instead of bare soil, and the FVC may be overestimated. Therefore, $NDVI_S$ and $NDVI_V$ were defined to be equal to 0.2 and 0.86, respectively (Ermida et al., 2020). Then, LSE was estimated by empirical equations using FVC for Landsat TM and OLI (Eq. (6.1) and 6.2) (Son & Thanh, 2018; Van De Griend & Owe, 1993).

$$FVC = \left(\frac{NDVI - NDVI_S}{NDVI_V - NDVI_S}\right)^2 \quad (5)$$

$$\varepsilon_{TM} = 0.004FVC + 0.986 \quad (6.1)$$

$$\varepsilon_{OLI} = 0.00149FVC + 0.986481 \quad (6.2)$$

$$T_S = \frac{T_B}{1 + (\lambda T_B/\rho)\ln\varepsilon} - 273.15 \quad (7)$$

Table 2
Landscape metrics adopted in this study.

Indicator	Description	Unit
Aggregation index (AI)	AI describes the agglomeration of individual landscape patches into a single clump/compact patch. It is calculated by number of like adjacence involving the corresponding class, divided by the maximum possible number of like adjacence, and multiplied by 100. Value range: $0 < AI < 100$ AI receives 0 when the considered path is totally disaggregated (or an independent patch). It increases the AI value when the patch is increasingly aggregated. AI achieves maxima of 100 when the patch is maximum aggregated (or a single, compact patch).	Percent
Largest patch index (LPI)	LPI presents the percentage of the homogeneous largest patch against the total landscape. It is estimated by the size (m^2) of the largest patch, divided by total landscape area (m^2), and multiplied by 100. Value range: $0 < LPI < 100$ LPI is approximately 0 when the largest patch of a landscape is too small (or the majority of this area is occupied by other landscapes). It increases proportionally with size of the largest patch index and reaches 100 when the entire area is covered by this single patch and this patch is also the largest patch.	Percent
Number of patches (NP)	NP is the quantity of single/independent patches of a specific landscape type. It represents the fragmentation of a landscape. A fragmented landscape is supposed to have a larger NP compared to the aggregated landscape because the patches combine into a single patch. Value range: $NP \geq 1$	None
Percentage of landscape (PLAND)	PLAND is the proportion of a specific landscape type (class) against total landscape area. It is estimated by total area of the considering class (m^2) divided by total landscape area (m^2) and multiplied by 100. Value range: $0 < PLAND < 100$ PLAND is 0 when the considering class does not exist in this landscape. It increases when this class increases its covering area, and PLAND reaches 100 when the whole landscape is occupied by this class.	Percent

*Notes: Suffixes "_U" and "_G" are added after each index to represent corresponding metrics for urban features and green spaces, respectively.

where, FVC is vegetation fraction; $NDVI_S$ and $NDVI_V$ are vegetation index of fully dense vegetation and bare soil, respectively; ε_{TM} and ε_{OLI} are land surface emissivity for Landsat TM and Landsat OLI; T_S is land surface temperature (°C); T_B is brightness temperature in Kelvin; λ is wavelength of emitted radiance (i.e., Landsat TM is band 6, λ_{B6}=11.5 μm, and Landsat OLI is band 10, λ_{B10}=10.89 μm); $\rho = hc/\sigma$, with ρ=1.438×10^{-2} Mk; ε is the land surface emissivity.

The surface urban heat island (SUHI) region was identified as a region with LST higher than an equation of average LST (μ) and standard deviation (σ) (Eq. (8)) (Wemegah et al., 2020). SUHI intensity (SUHII) was then calculated as the difference between a SUHI pixel and the average LST of rural areas (Eq. (9)).

$$LST > \mu_{LST} + 0.5\,\sigma \tag{8}$$

$$SUHII = LST_{SUHI} - LST_{Rural} \tag{9}$$

where, μ_{LST} is scene average LST; σ is standard deviation; SUHII is surface urban heat island intensity; LST_{SUHI} is a specific pixel where urban heat island phenomena occur; LST_{Rural} is average LST of the non-SUHI region.

3.5. Assessing effects of climate change and urbanization on SUHI

A bivariate correlation analysis and linear regression analysis between landscape metrics, extreme climate indices, and SUHII was implemented to explore influenced levels of considered variables to SUHI. The influenced level was quantified by the slope (β) magnitude from regression analysis, while the propensity of a variable was determined by the Pearson correlation coefficient (R). Additionally, we adopted principal component analysis (PCA) to explore the critically typical elements in each city, which may be eliminated by the strict statistical criteria of regression, such as meaningful level and multicollinearity. Yet, this elimination may lead to insufficient assessment from potential contributors. On the contrary, PCA solely reduces data dimension while it still respects individual contributions. PCA is particularly useful when working with a "wide" dataset, which observes many variables for each sample. Therefore, PCA is increasingly being used in environmental research as part of a modern school of analysis, for example, Awobona et al., (2020) and Loc et al., (2021).

4. Results

4.1. Trends in temperature and its extremes

Average temperature trends in BKK and HCM are shown in Fig. 2. The average mean, maximum, and minimum temperatures (Tmean, Tmax, Tmin) in BKK are generally higher than those in HCM. These parameters are significantly different between the two cities (P<0.01 obtained by t-test analysis). Although there are fluctuations over 30 years in both cities, the general trend is increasing average temperatures. More explicitly, the temperature in HCM is significantly rising (P<0.1). Whereas the warming effect in BKK is slightly positive compared to that in HCM, and this trend is insignificant over the observed period (P>0.1) (Fig. 2-A).

The Mann-Kendall test for temperature extremes indices revealed a similar tendency of rising for most indices except Minimum of TX (TXN) (Fig. 2-B). The maximum temperature indices, TXMEAN and TXX, have increased by less than 0.05 °C per decade for BKK and HCM. The increased magnitude of TX indices is not much different between the two locations. In contrast, the exacerbation in minimum temperature indices is relatively significant, especially for HCM (P<0.05). The increased magnitude and temperature difference between BKK and HCM, assessed by the magnitude of the trend slope, is undoubtedly greater. In BKK, the Min-based indices increased by 0.06 °C per decade (TNN) and 0.12 °C per decade (TNMEAN and TNX), respectively. These numbers are double in HCM with 0.23 °C per decade and 0.24 °C per decade for TNMEAN and TNN, respectively. The warmest trend was found in HCM relating to TNX, in which the increase was up to 0.3 °C per decade. During the last 30 years, BKK and HCM have shown climate change signals through the warming trends. The nocturnal warming is more obviously observed against daytime changes.

4.2. Urban expansion and alterations in landscape metrics

The general LULC classification obtained by the proposed classification framework with SVM classifier on Landsat imagery all achieved a high accuracy level, with an overall accuracy higher than 95% and Kappa coefficient greater than 0.94, which are suitable for urbanization analyses. The spatial distribution of urban areas in the two cities every five years starting from 1990 and their major urban expansion patterns are depicted in Fig. 3. The cities have experienced a continuous urban expansion over time. In 1990, BKK held 453.5 km^2 of built-up areas, which is ten times larger than the built-up area in HCM (43 km^2). The urban density at this base time was only 1.52% and 16.1% for HCM and

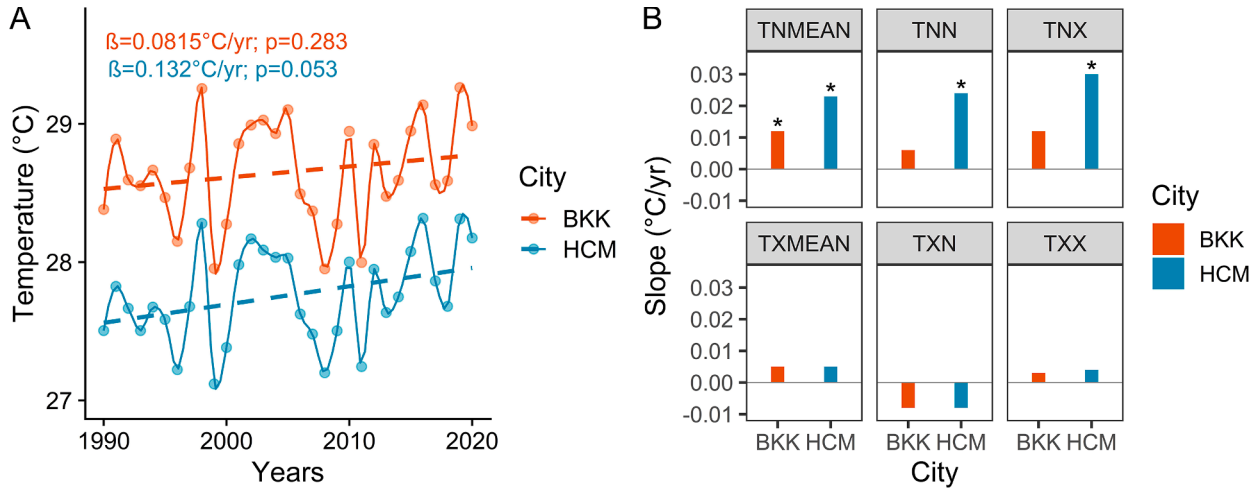

Fig. 2. Mean temperature trends in Bangkok and Ho Chi Minh City during 1990–2020. (A) Annual mean temperature and linear regression (dashed lines) show increasing trends. (B) Sen's slope presents the changing magnitude for temperature-based extreme indices. Symbol (*) indicates statistical significance.

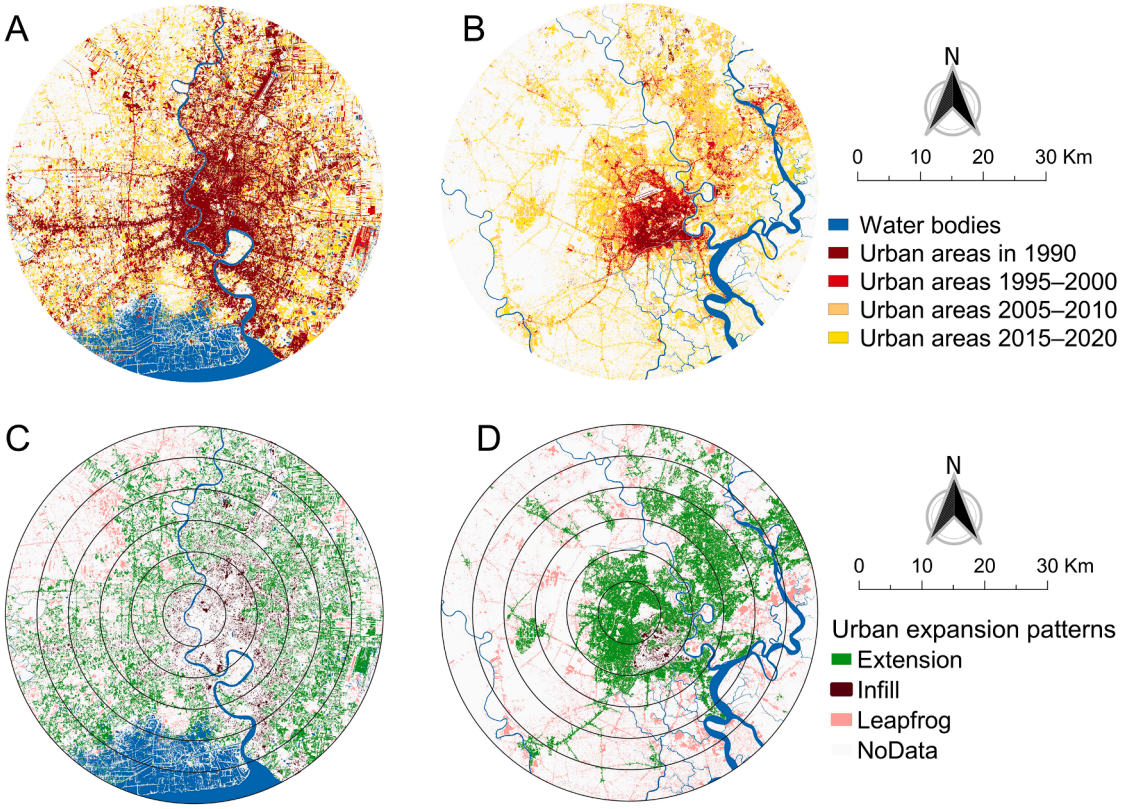

Fig. 3. Urban areas expanded over 1990–2020 in (A) BKK and (B) HCM. Urban expansion patterns throughout 30 years in (C) BKK and (D) HCM.

BKK, respectively. The disparities in urban scale and urban density have been rapidly narrowed across each subsequent period. At the end of the period, the gap in urban areas remained only 1.5 times, equivalent to 1,052.5 km^2 in BKK versus 682.5 km^2 in HCM. The urban density in HCM accounted for 10.1% in the middle of the period and then achieved 24.1% in 2020. BKK is always bigger than HCM regarding urban size, with its urban density of 20.4% (2005) and 37.4% (2020).

The total increased urban land throughout 30 years in HCM visibly expanded to about 639.5 km^2 (Fig. 3B), equal to an average AUGR of 48% per year. The urbanization was relatively rapid in the first 15 years, approximately 14.6–20% per year. The average AUGR then slowed down to a level of 5.2–8.9% per year. The primary urbanization form in HCM was an extension (70.7%), which tended to expand dramatically within 10 km and towards the northeast of the city center (Fig. 3D). The

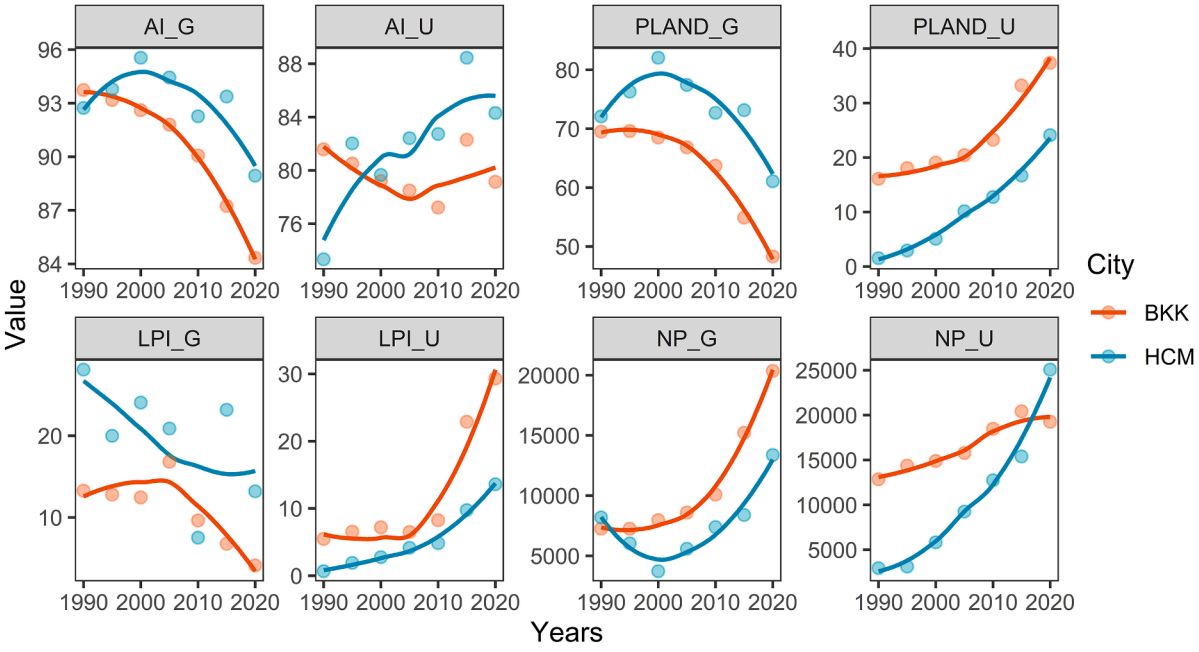

Fig. 4. Variations in average landscape metrics over the years for urban features and green spaces in BKK and HCM. For both cities, green spaces have declined in proportion, aggregation, and patch size, while the number of patches has increased. Unit of each indicator is shown in Table 2.

leapfrog pattern is mainly located outside the city core from 10 km outwards, accounting for 28.1% of the total urbanized area. Whereas the infill pattern humbly occupied 1.2% in the HCM city center area.

In BKK, the AUGR was relatively stable at a level of 4.6% per year, and it developed equally throughout the period (1.1–8.6% per year). The main urbanized form in this city was still an expansion pattern based on the developed areas (77.8%) that spanned most distances and directions (Fig. 3A-C). The leapfrog pattern area was one-half of the number held by HCM. It is highlighted that the infill urbanized pattern in BKK accounted for a relatively significant fraction of 8.1% of the total increased urban area.

The changes in landscape metrics (i.e., urban features and green spaces) during the urbanization process were then investigated and shown in Fig. 4. The percentage of the landscape for urban features (PLAND_U), representing the total urban area in both BKK and HCM tended to increase gradually. In contrast, the percentage of the landscape for green spaces (PLAND_G) showed a corresponding downtrend. At the end of the period, green spaces remained 61.1% and 48.3% in HCM and BKK, respectively. The landscape agglomeration was evaluated by the aggregation index (AI), while the landscape fragmentation was investigated by the largest patch index (LPI) and the number of patches (NP). These metrics together revealed that there was fragmentation and complexity for green spaces in these places. More explicitly, the green spaces aggregation (AI_G) and the largest patch index (LPI_G) gradually fell, and the number of patches (NP_G) climbed over time. The green spaces in BKK were mainly composed of narrowed areas and divided into smaller separated patches. A similar process also occurred for the urban green spaces in HCM. Yet, the fragmentation of green spaces in this city is less complex compared to that in BKK. The disparity in terms of urban agglomeration between these two cities was also observed. The number of urban patches (NP_U) in HCM has been higher than the number of patches in BKK since 2015. HCM exceeded BKK in the degree of urban aggregation (AI_U), where this index in HCM has been higher than that in BKK since the early 1990s. The landscape metrics of urban features and green spaces revealed a general process of urban agglomeration and green space fragmentation, in which BKK stands out for its urban areas fragmented by complex urban green spaces.

4.3. Escalation of LST and SUHI

The remote sensing-based estimation found that the two cities' surface temperatures have increasingly warmed. In HCM, the LST is generally warmer, about 0.15 °C per year, which is relatively higher than the annual increase in BKK estimated through 30 years (0.126 °C per year). When considering only LST, the BKK surfaces were generally hotter than that in HCM for every observation period. The disparity in average surface temperature frequently remained at a level of less than 0.5 °C. Yet, the maximum LST at some specific locations in HCM exceeded the values observed in BKK. These observations have been detected since 2005 (Fig. 5A) with anticipated linking to considerable urban development in terms of LPI shown in Fig. 4 above. For example, the max LST reached 39.8 °C in HCM, while the hottest pixel found in BKK in 2020 was only 36.8 °C.

The escalation of microclimate phenomena was obviously revealed through SUHI increases (Fig. 5B). The SUHI also shows an upward movement from 1990 to 2020, averaging 0.086 °C per decade and 0.46 °C per decade for BKK and HCM, respectively. The SUHI exacerbation in HCM is more significant than in BKK (Linear regression coefficient: R^2=0.76, P<0.01). Notably, the SUHII in HCM was lower than in BKK during the first 15 years; however, the situation has been in reverse since 2015. The SUHII of HCM has been approximately 0.55–0.69 °C higher compared to the microclimate magnitude in BKK. The max SUHII in the two cities has significantly risen and hit the highest record in 2020, at 9.8 °C (BKK) and 13.2 °C (HCM).

4.4. Association between SUHI and its controlling factors

Fig. 6 shows comprehensive matrices of correlation and regression slope indicating the associations and influences of the landscape metrics, urbanization, and temperature extreme indices on SUHII parameters (i.e., Average SUHI – UHIM, Maximum SUHI – UHIX, and Minimum SUHI – UHIN) in BKK and HCM. The relations of considered factors with SUHII parameters were roughly similar in HCM, but the effects were only intensive for UHIX and UHIN in BKK. The SUHII parameters on both BKK and HCM were significantly associated with urban agglomeration and urbanization, reflecting highly positive correlation coefficients (R) and slope values for LPI_U, NP_U, and PLAND_U. The second factor closely related to the SUHI rise was the shrinking and fragmentation of green spaces. The green space fragmentation-related metrics such as AI_G, LPI_G, and PLAND_G were highly negative relationships. More specifically, the green space changes in BKK are supposed to have much more impact on the SUHI severity than in HCM, presented by significant connections with green space metrics. For instance, the association

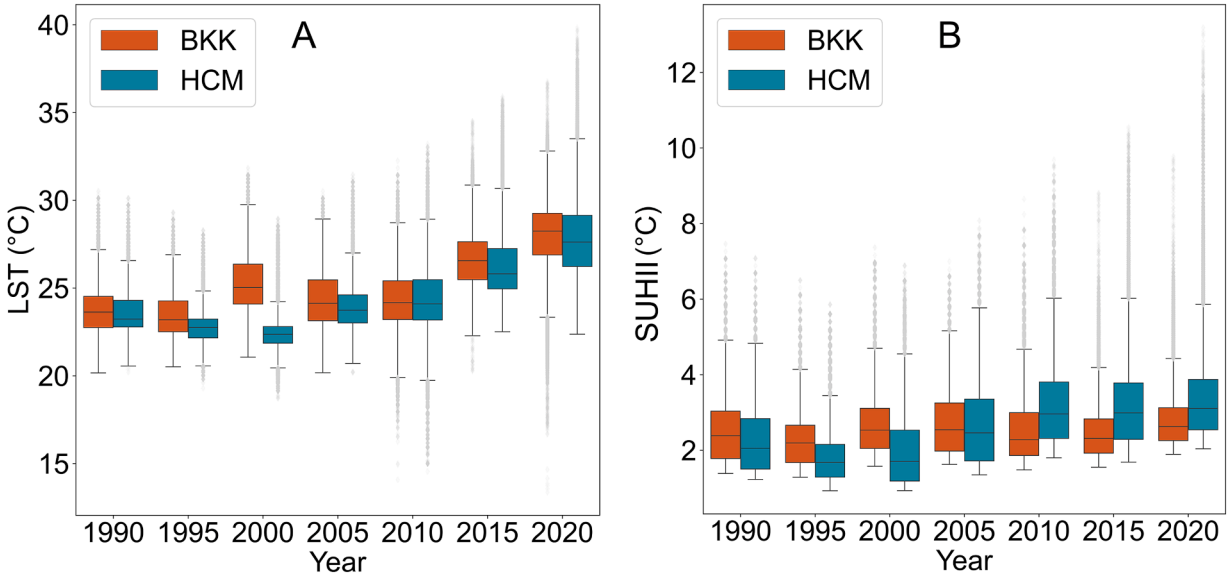

Fig. 5. Boxplots present changes of (A) LST and (B) SUHII in BKK and HCM over 30 years.

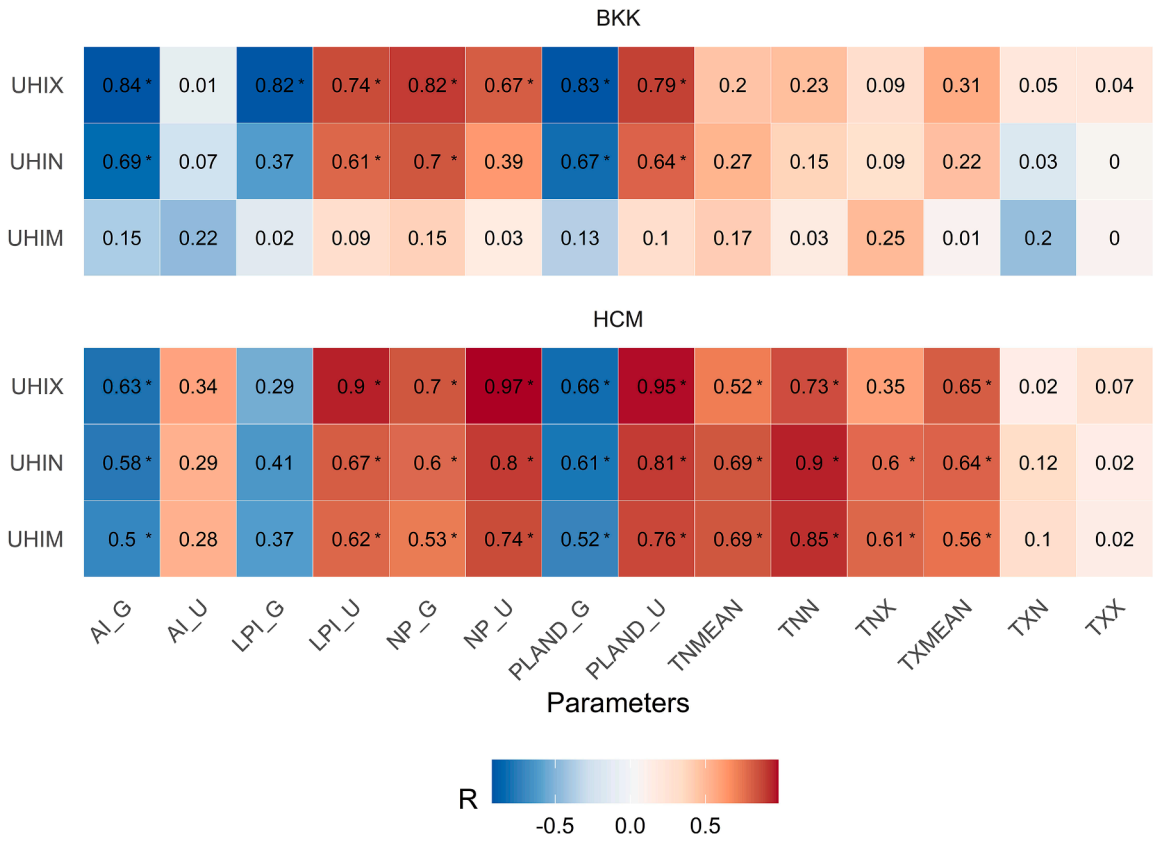

Fig. 6. Heatmaps show correlation coefficients and trend magnitude between landscape metrics and temperature extremes indices against SUHI parameters in BKK and HCM. Color tone presents trends of correlation analysis. Red and blue are proportional and inversely proportional correlations; the number is slope magnitude from linear regression. Symbol (*) indicates a statistically significant contributor ($P < 0.1$) to SUHI through regression analysis.

between LPI_G and UHIX in BKK is a markedly high β=0.82. In contrast, the correlation coefficient was at a moderate level of β=0.54 in HCM, and even insignificant through the regression analysis.

Regarding temperature extremes, although the SUHII in both cities has been more or less heated in line with the global warming trend as shown via positive associations, it varies widely in both cities. It is noteworthy that the increase in SUHII in HCM is more closely connected to climate change in terms of temperature severity than in BKK, particularly for TNN, TNX, and TNMEAN (β≥0.52). The lowest nighttime temperature (TNN) increase in HCM is strongly proportional to the SUHI intensity (β≥0.73). The daytime temperature (TXMEAN) also greatly contributes to warming the SUHI (β≥0.56). Whereas the temperature aspect of climate change impacts SUHI, in BKK it is moderate and low for most indicators, with β ≤ 0.31.

The PCA results for the individual city were summarized in Fig. 7 with the first two dimensions (Dim). Specifically, about 57.2% and 60.6% of variance are explained by the first dimension (Dim1 or PC1) for BKK and HCM, respectively. The PC1 was retained to represent the

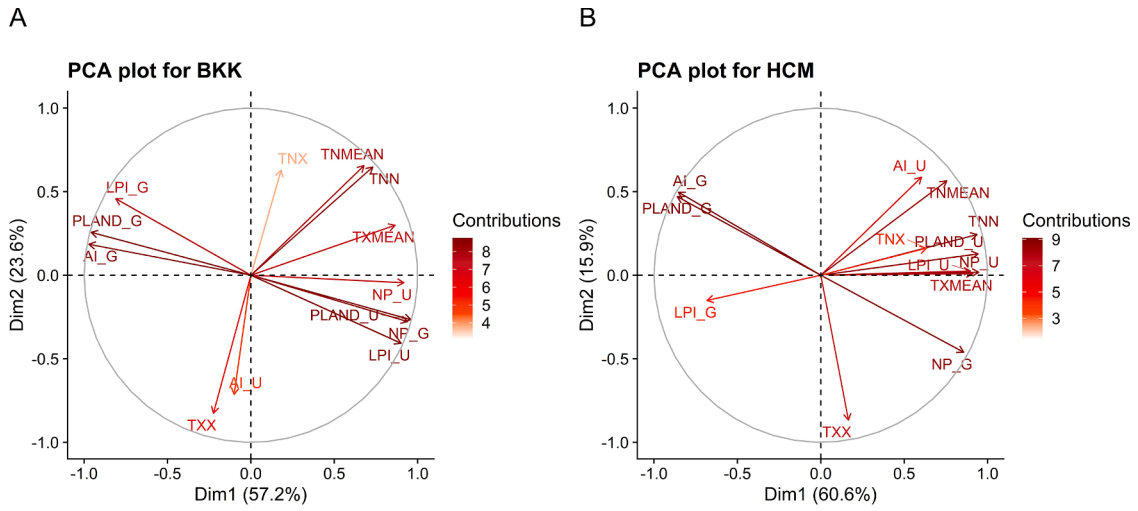

Fig. 7. Principal component analysis shows contributions of the latent variables into the first two components for (A) BKK and (B) HCM. The variable vectors approaching horizontal and vertical axes in turn contribute to PC1 and PC2. The vector length and color intensity are proportional to the contribution.

key elements influencing the SUHI in each city. Among the total 14 considered elements in BKK, eight elements significantly contribute to the formation of PC1, in which vectors approach the horizontal axis, including PLAND_U, PLAND_G, NP_U, NP_G, LPI_U, LPI_G, AI_G, and TXMEAN (Fig. 7A). Similarly, the PC1 in HCM is relatively similar to the PC1 in BKK, constructed by nine variables (Fig. 7B). However, the LPI_G is replaced by the other two climate change representing indices (TNMEAN and TNN).

5. Discussion

5.1. Rapid urban expansion along with climate change facilitate SUHI aggravation

BKK and HCM are dynamic cities from socioeconomic perspectives. A comparison between these two cities in various aspects was performed to illustrate the urbanization and climate change effects on SUHI. The research findings revealed that LULC changes are closely linked to changing thermal environments in both places. This influence even exceeds the impacts of climate change through warming severity. The effects of LULC changes through urban expansion and landscape metric alterations on LST escalation and SUHI formation found in this research were in line with those reported in other cities (Estoque & Murayama, 2017; Haiting et al., 2017). Specifically, the urban sprawl with shifts in landscape metrics is still the most significant contributor to SUHI severity against climate change, as indicated in the case of BKK, where climate change only has weak impacts (Fig. 6). Urban expansion is a principal LULC change in urban areas, which is also one of the major reasons for climate change by enhancing the emissions of greenhouse gasses into the atmosphere (Kachenchart et al., 2020). Urbanization directly leads to urban heat islands (i.e., surface and air UHI) by changing surface characteristics, anthropogenic heat, and alternations in urban morphology. Additionally, climate change also stimulates urban heat islands by variations in weather conditions, such as incoming radiation, cloud cover, and wind speed. Ultimately, urban growth and climate change jointly enhance urban heat islands (Chapman et al., 2017).

Both cities have also been confronting a relatively similar warming trend during the daytime, which is deemed to be influenced by general control from the same climate pattern and atmospheric circulations, as well as the comparable position of coastal deltas (as introduced in Section 2.1). Yet, the great dissimilarities in urban growth dynamics led to the big differences in the local heat environment, especially during nighttime, as prominent evidence for climate change in HCM. Higher nighttime temperature in HCM is also a vital sign that it has a problem with urban morphology since urban morphology is a main controlling mechanism for nighttime temperature. The different urbanization levels between BKK and HCM may result in significant variations in urban morphology, related building factors (e.g., sky-view factor, ventilation, and urban shading), and SUHI ultimately. The disparity in urban morphology should be further investigated to illuminate its impacts on SUHI in these cities.

In BKK, the temperature is stimulated by an extensive urban size with a lack of green and blue spaces, while SUHI in HCM is promoted by both rapid urbanization and climate change. The first component of PCA is to figure out the impacts of urban growth as significant core variables (Fig. 7). BKK holds a more extensive metropolitan scale, and the gap in urban scale between the two cities has been gradually narrowing. On the other hand, HCM is a more dynamic city with rapidly alternating urban areas and landscape metrics; the AUGR always exceeds BKK, especially in the early 21st century. Simultaneously, the dynamics of LULC in HCM are exacerbated by climate change through global warming, causing the city to heat up significantly. As a result, the magnitude of SUHI in HCM has been greater than in BKK, despite the fact that BKK has a higher LST.

It should be noted that the characteristics of the thermal environment in each city imply different meanings and considerations for citizens and urban managers. The higher LST in BKK is possibly linked to thermal comfort and power usage for cooling demand (Nguyen et al., 2021). In contrast, inhabitants in HCM are said to be more sensitive due to the increased intensity of SUHI. For example, when traveling around the city amid enormous temperature changes, they may get heatstroke and heat shock. Furthermore, the impacts of climate change are much more likely to increase this. It also suggests an urgent study direction in HCM on heat-related vulnerability for the residents under various scenarios, which would be particularly useful for national public-health initiatives.

5.2. Implications for long-term strategies

BKK and HCM have been experiencing rapid urbanization and SUHI formation. The thermal environment situation is expected to worsen as the cities continue to develop, exacerbated by the hot-humid tropical climate and climate change escalation. Thus, an insightful understanding and long-term strategies to mitigate SUHI for each city toward sustainable development are essential. Typically, the classic interventions to mitigate SUHI are to improve urban ventilation by ensuring the sky-view factor for canyons, to optimize natural cooling capacity through green and blue spaces, and to apply new materials in urban areas. Yet, the same measures may not be suitable for both cities since each city has its unique characteristics. BKK is in the mature stage, while HCM is just in the preliminary stages of development.

In particular, urbanization in BKK is presently dominated by extension and infill patterns with high urban density in the inner districts (Section 4.2). Thus, public green space plans, such as urban forests and large public parks, in these areas are difficult to implement. Green infrastructures such as integrated green spaces (e.g., rooftop garden, green wall, private garden, artificial wetland), and technical solutions (e.g., cool material roof, permeable pavement, cool material pavement) may be more appropriate (US EPA, 2008a, 2008b). The infill urbanization form is deemed to be hotter than the other two patterns (Zhang et al., 2021). Therefore, constructions between already urban areas need to be carefully considered as to whether they should be for construction or for green space conservation. These areas do not necessarily need to be planned as parks, but urban agriculture is also a solution worth considering for urban biodiversity and food security.

In HCM, the primary process is rapid urban expansion, which continuously expands the urban areas by extension and leapfrog patterns at urban fringes and towards connecting satellite cities (Fig. 3-B). Since early 2021, the three eastern districts of the city have been merged into one city directly under HCM, the first exceptional case in Vietnam. It will be expected to be more increasingly dynamic and expand in the future. At this stage, when the urban scale and new urban areas are still under control, urban governments should have a long-term vision toward sustainable urban development instead of “monotonic developments” that only focus on urban expansion and industrialization. A few issues should be noted, especially in the emerging urban areas of HCM, which are green space conservation and urban morphology standards. The intensive differences in nocturnal temperature in HCM compared to BKK (Section 4.1) are a critical sign of urban morphological problems. One of the biggest problems in HCM is the lack of synchronous construction leading to traffic congestion, adjoining houses, dense buildings, and urban slums. The compact urban areas prevent heat advection away from the city by ventilation, trapping it inside the urban infrastructures, and exacerbating SUHI (US EPA, 2008c). Therefore, spatial planning and urban morphology in this city can gradually eliminate current problems related to heat environment degradation and improve the city’s appearance. Simultaneously, HCM should incorporate climate change into the master plan as an important challenge to address throughout the development. Subsequently, there is appropriate design planning, not only for temperature changes and SUHI formation but also for the risk of sea-level rise, urban inundation, and tropical storms.

5.3. Methodological implications

In addition to its implications for urban and green space planning in the two cities, this study also opens up methodological implications for prompt LULC extraction as well as direction for improving LST prediction in future research.

5.3.1. Potential for automatic classification

The classification obtained from our proposed framework exceeds the high accuracy level (Section 4.2). It disclosed another option for automatic classification using GEE besides the current automatic approaches: index-thresholding extraction (Capolupo et al., 2020; Inman & Lyons, 2020) and supervised-based classification (Quintero et al., 2019; Xie et al., 2019). Our classification framework consisted of two parts, a self-automatic sampling procedure and a machine learning-based classifier of SVM. This sampling method is able to overcome the limitation of training data availability from MODIS products (presented by Xie et al., 2019), especially during the period before 2000. Whereas the supervised classification of SVM can improve the classification capability compared to the thresholding method, it is also replaceable with other MLC to enhance the classification for diverse applications.

5.3.2. Way forward for improving urban LST prediction

This study showcases the potential impacts of urbanization and climate change jointly in urban LST and SUHI exacerbation. Yet, the current predictive studies on LST that simulate the future LST are primarily based upon urban expansion and LULC change scenarios (Firozjaei et al., 2018; Mumtaz et al., 2020). Specifically, associations between LULC indices, urban patterns, and LST magnitude are investigated, and they are then adopted to predict LST magnitude. Although some auxiliary factors were also concerned with LST prediction research, e.g., slopes, elevation, accessibility to roads, and cool surfaces (Nurwanda & Honjo, 2019), these elements only support urban prediction. Furthermore, most of these studies ignored climate change impacts in LST prediction. It leads to insufficiently evaluating heat-related vulnerability in urban areas, while climate change also noteworthily contributes to LST and SUHI escalation as presented in our analysis (Section 4.4). Therefore, climate change impacts should be included in future predictive models to adequately quantify the increase in LST against the backdrop of increasingly pronounced and intense effects of climate change.

6. Conclusions

Previous studies on SUHI mainly focus on local impacts from LULC changes, urbanization, and surface alterations. In this study, we included climate change impact as an additional element in our assessment of SUHI in addition to urban expansion with shifts in landscape metrics to see how these aspects associate with thermal environmental changes. Each aspect was addressed in turn and the dynamics of each city were then revealed. To encapsulate, this study reached the following salient conclusions: in general, both BKK and HCM were considered two of the most dynamic cities in SEA in terms of urban development with dramatic transformations in urban areas, urbanization patterns, and landscapes, especially from urban vegetation shrinking. BKK has led in city size and urban density with a consistent growth rate, while HCM is a serious competitor with a rapid growth rate, particularly in the last decade. This made it possible to progressively close the distance between the two cities. Based on the results of temperature extremes, these cities have experienced the effects of climate change, which are particularly noticeable at night. Simultaneously, the degradation of the urban thermal environment was also confirmed via escalations of both surface temperature and SUHI. This aggravation was found to be mainly driven by urbanization-related elements and climate change as a background climate factor. Yet, it is prominent in HCM and has a significant contribution to local climate change. HCM is hence supposed to be a more vulnerable city due to combined impacts.

This study considered climate change as a return effect further amplifying the urban thermal environment, even though the forward effect of urbanization on near-surface temperature is widely accepted. This study also highlighted planning implications related to the unique characteristics of each city. The integrated solutions for combining green space types and high albedo materials in urban landscapes should be considered in the dense urban areas of BKK because of land fund constraints. Meanwhile, HCM needs to pay special attention to spatial planning, urban morphology, and green space restoration and conservation in newly developing urban areas. The two cities also need long-term strategies to increase resilience under the impact of far-reaching changes in the thermal environment and climate change, especially in Ho Chi Minh City. Our study also contributed to methodological merits through the applied methods, which showed the potential application to obtain LULC automatically based on GEE. The LST and SUHI predictions are expected to be ameliorated by adding climate change effects into the current models as a potential predictor.

Funding

This research received financial support from Petchra Pra Jom Klao Doctoral Scholarship for the Ph.D. program (09/2562) of King Mongkut's University of Technology Thonburi (KMUTT), the Joint Graduate School of Energy and Environment (JGSEE), and the Center of Excellence on Energy Technology and Environment (CEE), PERDO, Ministry of Higher Education, Science, Research and Innovation.

CRediT authorship contribution statement

Can Trong Nguyen: Conceptualization, Methodology, Software, Validation, Formal analysis, Visualization, Writing – original draft, Writing – review & editing. **Amnat Chidthaisong:** Conceptualization, Writing – review & editing, Supervision. **Atsamon Limsakul:** Conceptualization, Writing – review & editing. **Pariwate Varnakovida:** Conceptualization, Writing – review & editing. **Chaiwat Ekkawatpanit:** Conceptualization, Writing – review & editing. **Phan Kieu Diem:** Writing – review & editing. **Nguyen Thi Hong Diep:** Writing – review & editing.

Declaration of Competing Interest

The authors declare that they have no known competing financial interests or personal relationships that could have appeared to influence the work reported in this paper.

Acknowledgments

We would like to wholeheartedly thank the financial funders Petchra Pra Jom Klao Doctoral Scholarship of King Mongkut's University of Technology Thonburi (KMUTT), the Joint Graduate School of Energy and Environment (JGSEE), and the Center of Excellence on Energy Technology and Environment (CEE), PERDO, Ministry of Higher Education, Science, Research and Innovation for financial support to accomplish this research. Special thanks to the USGS and Google Earth Engine (GEE) platform for the freely accessible Landsat images and TerraClimate dataset used in this study. Finally, we express our gratitude to anonymous reviewers of this manuscript for their constructive comments and suggestions.

References

Abatzoglou, J. T., Dobrowski, S. Z., Parks, S. A., & Hegewisch, K. C. (2018). TerraClimate, a high-resolution global dataset of monthly climate and climatic water balance from 1958 to 2015. *Scientific Data, 5*, 1–12. https://doi.org/10.1038/sdata.2017.191

Akhtar, R. (2016). *Climate change and human health scenario in south and southeast asia.* Springer.

Artola, A. C., Bezanilla-Morlot, A., Taylor, M. A., Herrera, D. A., Martinez-Castro, D., Gouirand, I., et al. (2020). Evaluation of sixteen gridded precipitation datasets over the caribbean region using gauge observations. *Atmosphere, 11*(12). https://doi.org/10.3390/atmos11121334

Ascensão, F., Fahrig, L., Clevenger, A. P., Corlett, R. T., Jaeger, J. A. G., & Laurance, W. F. (2018). Environmental challenges for the belt and road initiative. *Nature Sustainability, 1*(5), 206–209. https://doi.org/10.1038/s41893-018-0059-3

Awobona, T. A., Adedapo, J. O., Emmanuel, J. O., Osunsina, O., Ogunsanwo, J. A., & Bolaji, O. W. (2020). Analysis of environmental factors determining the adoption of land management practices in guinea savanna agro-ecological zone of kaduna using principal component analysis (PCA). *Asian Journal of Advances in Agricultural Research, 14*(2), 18–28. https://doi.org/10.9734/ajaar/2020/v14i230127

Berliana, S., Susanti, S., Siswanto, I., Nurlatifah, B., Latifah, A., Witono, H., et al. (2021). Analysis of wet and dry season by using the palmer drought severity index (PDSI) over Java Island. In *, 2331. AIP Conference Proceedings*. https://doi.org/10.1063/5.0041843

Bimaganbetova, M., Memon, S. A., & Sheriyev, A. (2020). Performance evaluation of phase change materials suitable for cities representing the whole tropical savanna climate region. *Renewable Energy, 148*, 402–416. https://doi.org/10.1016/j.renene.2019.10.046

Can, N. T., Diep, N. T. H., & Iabchoon, S. (2021). Direction of urban expansion in the Bangkok Metropolitan area, Thailand under the impacts of a national strategy. *Vietnam Journal of Earth Sciences, 43*(3). https://doi.org/10.15625/2615-9783/16313

Can, N. T., Diep, N. T. H., Iabchoon, S., Varnakovida, P., & Minh, V. Q. (2019). Analysis of factors affecting urban heat island phenomenon in Bangkok Metropolitan area, Thailand. *VNU Journal of Science: Earth and Environmental Sciences, 35*(1), 53–62. https://doi.org/10.25073/2588-1094/vnuees.4355

Capolupo, A., Monterisi, C., & Tarantino, E. (2020). Landsat images classification algorithm (LICA) to automatically extract land cover information in google earth engine environment. *Remote Sensing, 12*(7). https://doi.org/10.3390/rs12071201

Carlson, T. C., & Ripley, D.a. (1997). On the relationship between NDVI, fractional vegetation cover, and leaf area index. *Remote Sensing of Environment, 62*, 241–252. https://doi.org/10.1016/S0034-4257(97)00104-1

Chapman, S., Watson, J. E. M., Salazar, A., Thatcher, M., & McAlpine, C. A. (2017). The impact of urbanization and climate change on urban temperatures: A systematic review. *Landscape Ecology, 32*(10), 1921–1935. https://doi.org/10.1007/s10980-017-0561-4

Cheng, L., Guan, D., Zhou, L., Zhao, Z., & Zhou, J. (2019). Urban cooling island effect of main river on a landscape scale in Chongqing, China. *Sustainable Cities and Society, 47*, Article 101501. https://doi.org/10.1016/j.scs.2019.101501

Congalton, R. G., & Green, K. (2009). Assessing the accuracy of remotely sensed data: Principles and practices. *The photogrammetric record* (2nd edi). Taylor & Francis Group. https://doi.org/10.1111/j.1477-9730.2010.00574_2.x. Vol. 2.

Dang, T. N., Honda, Y., Do, D. Van, Pham, A. L. T., Chu, C., Huang, C., et al. (2019). Effects of extreme temperatures on mortality and hospitalization in Ho Chi Minh City, Vietnam. *International Journal of Environmental Research and Public Health, 16*(3). https://doi.org/10.3390/ijerph16030432

Davtalab, J., Deyhimi, S. P., Dessi, V., Hafezi, M. R., & Adib, M. (2020). The impact of green space structure on physiological equivalent temperature index in open space. *Urban Climate, 31*, Article 100574. https://doi.org/10.1016/j.uclim.2019.100574

Diep, N. T. H., Korsem, T., Can, N. T., Phonphan, W., & Vo Quang, Minh. (2019). Determination of aquaculture distribution by using remote sensing technology in Thanh Phu district, Ben Tre province, Vietnam. *Vietnam Journal of Science, Technology and Engineering, 61*(2), 35–41. https://doi.org/10.31276/VJSTE.61(2).35-41

Ermida, S. L., Soares, P., Mantas, V., Göttsche, F. M., & Trigo, I. F. (2020). Google earth engine open-source code for land surface temperature estimation from the landsat series. *Remote Sensing, 12*(9), 1–21. https://doi.org/10.3390/RS12091471

Estoque, R. C., & Murayama, Y. (2015). Intensity and spatial pattern of urban land changes in the megacities of Southeast Asia. *Land use policy, 48*, 213–222. https://doi.org/10.1016/j.landusepol.2015.05.017

Estoque, R. C., & Murayama, Y. (2017). Monitoring surface urban heat island formation in a tropical mountain city using Landsat data (1987–2015). *ISPRS Journal of Photogrammetry and Remote Sensing, 133*, 18–29. https://doi.org/10.1016/j.isprsjprs.2017.09.008

Estoque, R. C., Murayama, Y., & Myint, S. W. (2017). Effects of landscape composition and pattern on land surface temperature: An urban heat island study in the megacities of Southeast Asia. *Science of the Total Environment, 577*, 349–359. https://doi.org/10.1016/j.scitotenv.2016.10.195

Fall, S., Niyogi, D., Gluhovsky, A., Pielke, R. A., Kalnay, E., & Rochon, G. (2010). Impacts of land use land cover on temperature trends over the continental United States: Assessment using the North American regional reanalysis. *International Journal of Climatology, 30*(13), 1980–1993. https://doi.org/10.1002/joc.1996

Fan, P., Ouyang, Z., Nguyen, D. D., Nguyen, T. T. H., Park, H., & Chen, J. (2019). Urbanization, economic development, environmental and social changes in transitional economies: Vietnam after Doimoi. *Landscape and Urban Planning, 187*(October), 145–155. https://doi.org/10.1016/j.landurbplan.2018.10.014

Firozjaei, M. K., Kiavarz, M., Alavipanah, S. K., Lakes, T., & Qureshi, S. (2018). Monitoring and forecasting heat island intensity through multi-temporal image analysis and cellular automata-Markov chain modelling: A case of Babol city, Iran. *Ecological Indicators, 91*(January), 155–170. https://doi.org/10.1016/j.ecolind.2018.03.052

Foga, S., Scaramuzza, P. L., Guo, S., Zhu, Z., Dilley, R. D., Beckmann, T., et al. (2017). Cloud detection algorithm comparison and validation for operational landsat data products. *Remote Sensing of Environment, 194*(2017), 379–390. https://doi.org/10.1016/j.rse.2017.03.026

Güçlü, Y. S. (2018). Multiple şen-innovative trend analyses and partial Mann-Kendall test. *Journal of Hydrology, 566*(September), 685–704. https://doi.org/10.1016/j.jhydrol.2018.09.034

Haiting, W., Zhang, Y., Tsou, J., & Li, Y. (2017). Surface urban heat island analysis of Shanghai (China) based on the change of land use and land cover. *Sustainability, 9*(1538), 1–22. https://doi.org/10.3390/su9091538

Harun, Z., Reda, E., Abdulrazzaq, A., Abbas, A. A., Yusup, Y., & Zaki, S. A. (2020). Urban heat island in the modern tropical Kuala Lumpur: Comparative weight of the different parameters. *Alexandria Engineering Journal, 59*(6), 4475–4489. https://doi.org/10.1016/j.aej.2020.07.053

He, B. J., Ding, L., & Prasad, D. (2020). Urban ventilation and its potential for local warming mitigation: A field experiment in an open low-rise gridiron precinct. *Sustainable Cities and Society, 55*(December 2019), Article 102028. https://doi.org/10.1016/j.scs.2020.102028

Henderson, R. M., Reinert, S. A., Dekhtyar, P., & Migdal, A. (2018). *Climate change in 2018 : Implications for business*. Harvard Business School Publishing.

Hong Diep, N. T., Nguyen, C. T., Diem, P. K., Hoang, N. X., & Kafy, A.- Al (2021). Assessment on controlling factors of urbanization possibility in a newly developing city of the Vietnamese Mekong delta using logistic regression analysis. *Physics and Chemistry of the Earth, Parts A/B/C, 103065*, Article 103065. https://doi.org/10.1016/j.pce.2021.103065

Inman, V. L., & Lyons, M. B. (2020). Automated inundation mapping over large areas using landsat data and google earth engine. *Remote Sensing*, 1–12. https://www.mdpi.com/2072-4292/12/8/1348.

IPCC. (2018). Global warming of 1.5 °C: Summary for Policymakers. In Masson-Delmotte V., Zhai P., Pörtner H.-O., Roberts D., Skea J., Shukla P. R., Pirani A., Okia W. M., Péan C., Pidcock R., Connors S., Matthews J. B. R., Chen Y., Zhou X., Gomis M. I., Lonnoy E., Maycock T., Tignor M., & Waterfield T., (Eds.), *IPCC-Summary for Policymakers*. Intergovernmental Panel on Climate Change. https://doi.org/10.1017/CBO9781107415324.

Iping, A., Kidston-Lattari, J., Simpson-Young, A., Duncan, E., & McManus, P. (2019). (*Re*) presenting urban heat islands in Australian cities: A study of media reporting and implications for urban heat and climate change debates. *Urban Climate, 27*, 420–429. https://doi.org/10.1016/j.uclim.2018.12.014

Kachenchart, B., Kamlangkla, C., Puttanapong, N., & Limsakul, A. (2020). Urbanization effects on surface air temperature trends in Thailand during 1970-2019. *Environmental Engineering Research, 26*(5), Article 200378. https://doi.org/10.4491/eer.2020.378

Kawamura, M., Jayamanna, S., & Tsujiko, Y. (1996). Change detection using relative atmospheric correction of satellite images at different times. In K. Kraus, & P. Waldhausl (Eds.), *Technical commission VII: Resource and environmental monitoring* (pp. 321–326). ISPRS Congress. https://doi.org/10.1016/j.jamda.2013.04.003.

Kendall, M. G. (1975). *Rank correlation methods, edition* (4th ed.). Charles Griffin.

Khamchiangta, D., & Dhakal, S. (2019). Physical and non-physical factors driving urban heat island: Case of Bangkok metropolitan administration, Thailand. *Journal of Environmental Management, 248*(March), Article 109285. https://doi.org/10.1016/j.jenvman.2019.109285

Knutson, T., Kossin, J. P., .Mears, C., Perlwitz, J., & Wehner, M. F. (2017))(. Detection and attribution of climate change. In D. J. Wuebbles, D. W. Fahey, K. A. Hibbard, D. J. Dokken, B. C. Stewart, & T. K. Maycock (Eds.), *Climate science special report: Fourth National Climate Assessment* (Vol. 1, pp. 112–132). https://doi.org/10.7930/J0J964J6.

Kostianoy, A. G., .Soloviev, D. M., & .& Pešić, V. (2020). Application of google earth in mapping intermittent rivers of montenegro. *Handbook of Environmental Chemistry*, 93, 253–263. https://doi.org/10.1007/698_2020_488.

Loc, H. H., Park, E., Thu, T. N., Diep, N. T. H., & Can, N. T. (2021). An enhanced analytical framework of participatory GIS for ecosystem services assessment applied to a Ramsar wetland site in the Vietnam Mekong Delta. *Ecosystem Services, 48*(April 2020), Article 101245. https://doi.org/10.1016/j.ecoser.2021.101245

Lowe, S. A. (2016). An energy and mortality impact assessment of the urban heat island in the US. *Environmental Impact Assessment Review, 56*, 139–144. https://doi.org/10.1016/j.eiar.2015.10.004

Mann, H. B. (1945). Nonparametric tests against trend. *Econometrica: Journal of the Econometric Society*, 245–259.

McGarigal, K., Cushman, S. A., & .& Ene, E. (2012). *FRAGSTATS v4: Spatial pattern analysis program for categorical and continuous maps. Computer software program produced by the authors at the University of Massachusetts*.

Min, Z., Cheng, W., Zhou, C., Li, M., Huang, K., & Wang, N. (2018). Assessing spatiotemporal characteristics of urbanization dynamics in southeast Asia using time series of DMSP/OLS nighttime light data. *Remote Sensing, 10*(47), 1–20. https://doi.org/10.3390/rs10010047

Mumtaz, F., Tao, Y., Leeuw, G. De, Zhao, L., Fan, C., Elnashar, A., et al. (2020). Modeling spatio-temporal land transformation and its associated impacts on land surface temperature (LST). *Remote Sensing, 12*(18). https://doi.org/10.3390/RS12182987

National Research Council.. (2012). Climate change: Evidence, impacs, and choices. *National Academy of Sciences*. https://doi.org/10.1017/CBO9781139095723.023

Nguyen, C. T., Chidthaisong, A., Diem, P. K., & Huo, L. (2021a). A modified bare soil index to identify bare land features during agricultural fallow-period in southeast asia using landsat 8. *Land, 10*(231), 1–17. https://doi.org/10.3390/land10030231

Nguyen, C. T., Diep, N. T. H., & Diem, P. K. (2021b). Factors affecting urban electricity consumption: A case study in the Bangkok metropolitan area using an integrated

approach of earth observation data and data analysis. *Environmental Science and Pollution Research, 28*, 12056–12066. https://doi.org/10.1007/s11356-020-09157-6
Noi, P. T., & Kappas, M. (2018). Comparison of random forest, k-nearest neighbor, and support vector machine classifiers for land cover classification using sentinel-2 imagery. *Sensors, 18*(18). https://doi.org/10.3390/s18010018
Nurwanda, A., & Honjo, T. (2019). The prediction of city expansion and land surface temperature in Bogor city. *Indonesia. Sustainable Cities and Society, 52*, 2020. https://doi.org/10.1016/j.scs.2019.101772
Otsu, N. (1979). A threshold selection method from gray-level histograms. *IEEE Trans. Syst. Man Cybern, 9*(1), 62–66.
Pakarnseree, R., Chunkao, K., & Bualert, S. (2018). Physical characteristics of Bangkok and its urban heat island phenomenon. *Building and Environment, 143*(February), 561–569. https://doi.org/10.1016/j.buildenv.2018.07.042
Parent, J. (2009). *Urban landscape analysis tool. department of natural resources management and engineering*. University of Connecticut.
Quang, D. Van, Kusaka, H., & Ho, Q. B. (2016). Impact of future urbanization on temperature and thermal comfort index in a developing tropical city: Ho Chi Minh City. *Urban Climate, 17*, 20–31. https://doi.org/10.1016/j.uclim.2016.04.003
Quintero, N., Viedma, O., Urbieta, I. R., & Moreno, J. M. (2019). Assessing landscape fire hazard by multitemporal automatic classification of landsat time series using the Google Earth Engine in West-Central Spain. *Forests, 10*(6). https://doi.org/10.3390/f10060518
Santamouris, M. (2020). Recent progress on urban overheating and heat island research. Integrated assessment of the energy, environmental, vulnerability and health impact. Synergies with the global climate change. *Energy and Buildings, 207*, Article 109482. https://doi.org/10.1016/j.enbuild.2019.109482
Sein, K. K., .Chidthaisong, A., & Oo, K. L. (.(2018)). Observed trends and changes in temperature and precipitation extreme indices over Myanmar. In *atmosphere* (Vol. 9, Issue 12). https://doi.org/10.3390/atmos9120477.
Son, N. T., Chen, C., Chen, C., Thanh, B., & Vuong, T. H. (2017). Assessment of urbanization and urban heat islands in Ho Chi Minh City, Vietnam using landsat data. *Sustainable Cities and Society, 30*, 150–161. https://doi.org/10.1016/j.scs.2017.01.009
Son, N. T., & Thanh, B. X. (2018). Decadal assessment of urban sprawl and its effects on local temperature using landsat data in Cantho city, Vietnam. *Sustainable Cities and Society, 36*(2018), 81–91. https://doi.org/10.1016/j.scs.2017.10.010
Srivanit, M. (2012). Assessing the impact of urbanization on urban thermal environment : A case study of bangkok metropolitan. *International Journal of Applied Science and Technology, 2*(7), 243–256.
Susanti, I., Sipayung, S. B., Siswanto, B., Maryadi, E., Latifah, H., Nurlatifah, A., et al. (2021). Implications of extreme events on the water balance in Java. In *AIP Conference Proceedings* (p. 2331). https://doi.org/10.1063/5.0042006
TMD. (2015). *The climate of Thailand*. http://www.tmd.go.th/en/archive/thailand_climate.pdf.
Tucker, C. J. (1979). Red and photographic infrared linear combinations for monitoring vegetation. *Remote Sensing of Environment, 8*(2), 127–150. https://doi.org/10.1016/0034-4257(79)90013-0
United Nations. (2018). *The world's cities in 2018: Data booklet*. population division, department of economic and social affairs, United Nations.
United Nations. (2019). *World urbanization prospects 2018: Highlights*. United Nations, department of economic and social affairs, population division. https://population.un.org/wup/.
US EPA. (2008a). Cool Roofs. *Reducing urban heat islands : Compendium of strategies*. Washington, DC: U.S. Environmental Protection Agency.
US EPA. (2008b). Green Roofs. *Reducing urban heat islands: Compendium of strategies*. Washington, DC: U.S. Environmental Protection Agency.
US EPA. (2008c). Urban heat island basics. *Reducing urban heat islands: Compendium of strategies*. Washington, DC: U.S. Environmental Protection Agency.
Van De Griend, A. A., & Owe, M. (1993). On the relationship between thermal emissivity and the normalized difference vegetation index for natural surfaces. *International Journal of Remote Sensing, 14*(6), 1119–1131. https://doi.org/10.1080/01431169308904400
Van, T. T., & Bao, H. D. X. (2015). Characteristics of Urban Thermal Environment from Satellite Remote Sensing Data in Ho Chi Minh City, Vietnam. *Proceedings of the 1st International Electronic Conference on Remote Sensing*, 1–7. https://doi.org/10.3390/ecrs-1-f003
Van, T. T., Bao, H. D. X., Phuong, D. T. K., Mai, N. T. T., & Nhung, D. T. M. (2017). Characteristics of thermal environment and change detection of the surface urban heat island in the Northern part of Ho Chi Minh city. *Can Tho University Journal of Sciene, 49*(A), 11–20. https://doi.org/10.22144/jvn.2017.002
Wemegah, C. S., Yamba, E. I., Aryee, J. N. A., Sam, F., & Amekudzi, L. K. (2020). Assessment of urban heat island warming in the greater accra region. *Scientific African, 8*. https://doi.org/10.1016/j.sciaf.2020.e00426
Xie, S., Liu, L., Zhang, X., Yang, J., Chen, X., & Gao, Y. (2019). Automatic land-cover mapping using landsat time-series data based on google earth engine. *Remote Sensing, 11*(24). https://doi.org/10.3390/rs11243023
Xu, H. (2006). Modification of normalised difference water index (NDWI) to enhance open water features in remotely sensed imagery. *International Journal of Remote Sensing, 27*(14), 3025–3033. https://doi.org/10.1080/01431160600589179
Yamane, T. (1967). *Elementary sampling theory* (1st edition). Prentice Hall.
Yaung, K. La, Chidthaisong, A., Limsakul, A., Varnakovida, P., & Can, N. T. (2021). Land use land cover changes and their effects on surface air temperature in Myanmar and Thailand. *Sustainability, 13*(19), 1–21. https://doi.org/10.3390/su131910942
Zhang, Xinmin, Estoque, R. C., Murayama, Y., & Ranagalage, M. (2021). Capturing urban heat island formation in a subtropical city of China based on Landsat images: Implications for sustainable urban development. *Environmental Monitoring and Assessment, 193*(3), 1–13. https://doi.org/10.1007/s10661-021-08890-w
Zhang, Xuebin. (2009). *Climate Change Indices*. Expert team on climate change detection and indices (ETCCDI). http://etccdi.pacificclimate.org/list_27_indices.shtml.